ac susceptibility studies of intra- and intergrain properties of high-J_c Bi-2212 wires

Chiara Tarantini,* Temidayo Abiola Oloye, S. Imam Hossain, Fumitake Kametani, Jianyi Jiang, Eric E. Hellstrom, and David C. Larbalestier

Applied Superconductivity Center, National High Magnetic Laboratory, Florida State University, Tallahassee, Florida 32310, USA

(Received 5 October 2022; revised 8 December 2022; accepted 9 December 2022; published 9 January 2023)

$Bi_2Sr_2CaCuO_x$ (Bi-2212) is the only high-T_c superconductor (HTS) available as a multifilamentary round wire with multiple architectures and it is a very promising conductor for the realization of high-field applications. Despite their relatively simple wire fabrication by the powder-in-tube technique, Bi-2212 wires require a tightly controlled overpressure heat treatment (HT) with a multiparameter time-temperature schedule to achieve high critical current density, J_c. The variation of these HT parameters, changes in the wire design, wire diameter, and powder quality can lead to variations in both the microstructure and the superconducting performance. Particularly noticeable are variations in J_c performance and degree of filament bridging. In this work, we focus on the use of different magnetic characterization techniques to estimate the bridging level and assess the balance of intergrain and intragrain superconducting properties including the irreversibility field (H_{irr}) and the pinning energy (U_o) in differently processed wires. Regardless of the actual bridging level, we find that the supercurrent flows at the filament bundle level, not just at the individual filament level. Moreover, using ac susceptibility we identify two distinct supercurrent contributions, one related to the intragrain and one to the intergrain properties, whose irreversibility fields are different but without large sample-to-sample variation. Moreover, an additional component of intragrain pinning mechanism becomes effective at low temperatures with positive effects also on the intergrain performance. The work clearly shows that detailed magnetic characterizations can become valuable tools to investigate the performance of differently processed Bi-2212 wires, correlating their microstructure and overall transport J_c, to obtain a deeper understanding of the causes of performance variation and paths to achieve further improvement.

DOI: 10.1103/PhysRevMaterials.7.014802

I. INTRODUCTION

The interest in Bi-2212 wires notably increased in the last decade, making it one of the most promising high-T_c superconductor (HTS) conductors for high-field applications, such as accelerator, NMR, and research magnets. This was driven by a sudden performance advance generated by the introduction of an innovative overpressure heat treatment (OPHT) leading to a manyfold improvement in J_c [1]. Moreover, Bi-2212 is the only HTS round wire, making it particularly suitable for magnets, as demonstrated by the fabrication of solenoid magnets, racetracks made with Rutherford cables, and canted-cosine-theta dipoles [2–5].

Bi-2212 wires have an unusual local biaxially textured microstructure generated during the solidification step in the OPHT. Such texturing is what suppresses the degrading effects of weak links typical of high-angle grain boundaries (GBs) in HTS [6]. Because of the more than 1000 filaments, and because of the rotation of the average c-axis direction along each filament, Bi-2212 behaves as a macroscopically isotropic conductor [1,6]. Another microstructural feature of Bi-2212 wires is the development during solidification of filament bridges (thin Bi-2212 grains connecting filaments) or filament merging (when two or more initially discrete filaments form a larger element) [7]. Before OPHT was implemented, bridging was believed to be essential to obtaining high J_c to overcome the current-limiting effects of gas bubbles that subdivided the filaments [8–10]. Although mechanical deformation can be used to reduce the bubble presence and to increase the Bi-2212 density [11–13], the best J_c performance is obtained by OPHT, which hydrostatically shrinks the bubbles to practically zero density [1,14]. OPHT is a multistep heat treatment (HT) typically performed at 50 bar, with a partial pressure of oxygen of 1 bar, as described in Ref. [15]. The effects of all the HT parameters are not yet fully understood but it was demonstrated that the time in the melt ($t_{melt} = t_{872\,^\circ C\downarrow} - t_{884\,^\circ C\uparrow}$, with $t_{884\,^\circ C\uparrow}$ and $t_{872\,^\circ C\downarrow}$ being the times at which Bi-2212 starts melting on heating and starts solidifying on cooling, respectively) is a critical parameter. In particular, increasing t_{melt} increases the filament bridging, causing large variation in the microstructure and J_c performance [16].

Some important questions for Bi-2212 are still only partially answered. Amongst these are (1) Is filament bridging good or bad for J_c in OPHT-ed wires? (2) Does the long-range transport current percolate through these bridges? (3) Is the J_c (defined by I_c divided by the Bi-2212 cross-section) variation primarily due to connectivity or to changes in vortex pinning performance and how might we answer this question? About question 1, it is clear that filament bridging is an undesirable feature for hysteresis loss [17,18]; however, wire twisting can

*Corresponding author: tarantini@asc.magnet.fsu.edu

noticeably reduce the hysteresis losses without J_c degradation. With respect to the J_c magnitude, some level of bridging could overcome local filament blockage or cross-sectional variation (sausaging). However, strong bridging can also compromise the biaxial texture [16]. This suggests that a compromise between bridging advantages and disadvantages has to be found. About questions 2 and 3, although there are several studies suggesting that at least some bridges do carry current (see for instance [17,18]), large variations of J_c are likely determined by variable connectivity [19]. Thus, evaluating the scale of supercurrent percolation, the connectivity variation and changes in pinning efficiency in OPHT Bi-2212 round wires with different performance is highly valuable. In particular, we will focus on dc and ac magnetic susceptibilities, the first to evaluate the low-field shielding volume, the latter to investigate connectivity, the irreversibility field $H_{\rm irr}$, and the pinning energies U_0 under dc field, H_{dc}.

ac susceptibility characterization is a very versatile technique [20] widely used to study granularity in polycrystalline samples in the early days of HTS [21–23] but also more recently to investigate the iron-based superconductors [24,25]. In fact, double transitions in the real part of the first harmonic χ_1 and the presence of two peaks in its imaginary part provide information about intragrain and intergrain supercurrents [26,27]. Moreover, investigating the amplitude and frequency dependences of these transitions under variable ac field, H_{ac}, allows determination of the irreversibility field [28] and the pinning energy [22,29]. Although ac susceptibility has been performed before on Bi-based superconductors, they were mostly focused on 2223 [27,30–34] because of its better performance in tapes prior to OPHT of Bi-2212 [30,35,36]. However, ac susceptibility has never been performed on the modern, multifilamentary, OPHT round wires investigated here. We do note, however, that the complex structure of Bi-2212 wires can lead to several possible current paths: in fact, the normal Ag matrix can contribute eddy current signals, whereas Bi-2212 contributions can come from grains, filaments, filament bundles, or the entire wire. We will show that the effect of the Ag matrix can be strongly suppressed by proper experimental conditions, and we will demonstrate that the Bi-2212 contributions are limited to grains and bundles (each constituted, in the present case, by 85 filaments).

II. EXPERIMENT

A. Samples and preliminary characterizations

We used a Bi-2212 wire with an 85×18 restack design (pmm190425, constituted of 18 bundles with 85 filaments each) made with Engi-Mat precursor powder (LXC-09). Two wire diameters were employed, 1 and 1.2 mm, leading to densified average filament diameters prior to melting of 11.6 and 13.9 μm, respectively. In order to change the microstructure and wire performance, we heat treated the wires at a maximum temperature, $T_{\rm max}$, of 886 °C but we altered the cooling rate after cooling to 876 °C ($T_{\rm max}$–10 °C; see Ref. [15] for comparison). Three different cooling rates were employed: 1, 2.5, and 5 °C/h, generating six different samples whose main properties are summarized in Table I. Preliminary characterizations included transport measurements at 4.2 K in the 5–15-T field range and wire cross sections. We found a relatively small sample-to-sample variation in the transport J_c. The field dependence, estimated as $J_c \propto H^{-\alpha}$, shows α values ranging between 0.26 and 0.31, compatible with a previous report [19], where J_c was varying by a factor 5. The most obvious difference in the samples investigated here is in the J_c magnitude that, at 4.2 K and 5 T, ranges from 4982 to 4757 A/mm^2 in the 1-mm wires, and from 5236 to 4274 A/mm^2 in the 1.2-mm wires. Lower J_c values are expected with decreasing filament diameter, perhaps because of greater filament sausaging and also because of greater filament bridging developed during OPHT. Indeed, the filament bridging did become more marked with increasing $t_{\rm melt}$. Figure 1 shows two threshold images of the Bi-2212 phase obtained from the wire cross sections after HT with cooling rates of 1 and 5 °C/h: the perimeters of discrete elements in the cross sections are marked in gray to highlight the different level of bridging. In fact, they clearly show that, at 1 °C/h, many filaments are joined by Bi-2212 bridges, thus creating large filament clusters which, in some cases, comprise more than half of the filaments inside a bundle [many filaments are physically connected in Fig. 1(top)]. In contrast, at 5 °C/h, most elements remain individual filaments with just a few clusters of two or three filaments [Fig. 1(bottom)].

TABLE I. Summary of the main sample properties: wire diameter, heat treatment (HT) cooling rate, time in the melt, and transport J_c evaluated at 4.2 K and 5 T.

Wire diameter (mm)	HT cooling rate (°C/h)	$t_{\rm melt}$ (h)	Transport J_c (4.2 K, 5 T) (A/mm^2)
1	1.0	5.24	4982
	2.5	2.84	4743
	5.0	2.04	4757
1.2	1.0	5.24	5236
	2.5	2.84	4674
	5.0	2.04	4274

B. Magnetic characterizations

dc magnetic characterizations were performed in a Quantum Design MPMS-5 superconducting quantum interference device (SQUID) magnetometer using typically 4-mm sample lengths with field configurations both parallel and perpendicular. They were cooled down in zero field and then measured warming up in a small $\mu_0 H_{dc} = 1$ mT.

ac susceptibility was performed in a Quantum Design 9 T PPMS system, mainly with wires in the perpendicular configuration to induce shielding currents along the wires, which is the most relevant condition for applications, which require long-range transport current. Two 1.2-mm samples were selected for this investigation, which are the higher- and lower-J_c wires within this sample set (see Table I). We varied $\mu_0 H_{ac}$ between 0.1 and 1.5 mT, the frequency f between 13 and 757 Hz, while $\mu_0 H_{dc}$ was applied up to 9 T.

Because of the complexity of some of the results and their analysis, the results will be presented, analyzed, and explained one by one.

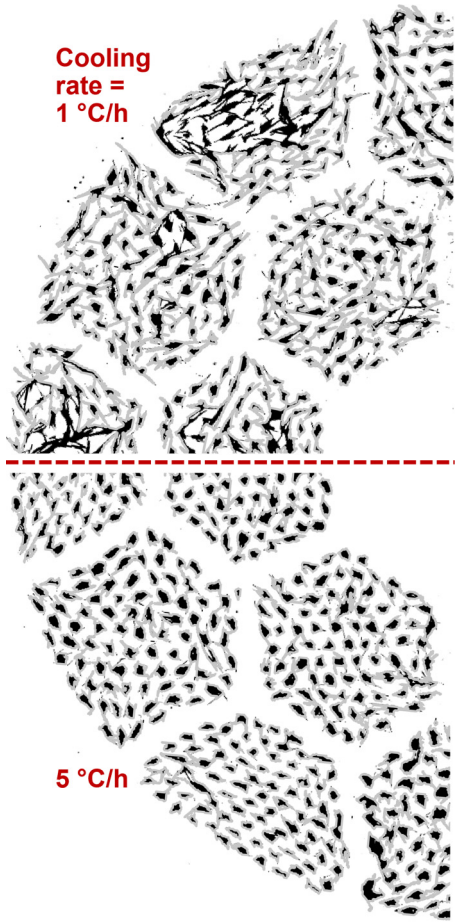

FIG. 1. Threshold images of the Bi-2212 phase; shown are 1/4 of the Bi-2212 wire cross sections (1.2-mm diameter) after heat treatments with different cooling rates at 1 (top) and 5 °C/h (bottom). The perimeters of discrete elements in the cross section are colored gray to highlight the different filament bridging behavior.

III. RESULTS AND ANALYSIS

A. dc magnetic characterization

Because of our interest in the superconducting phase, the data obtained in the SQUID magnetometer were initially analyzed assuming that the signals arose from individual, not-connected filaments (as is typically done in Bi-2212 conductors, the total filament area and the average filament diameter were estimated after an overpressure (OP) densification before melting [15]). The filaments were assumed cylindrical and the demagnetization factors were taken into account accordingly to their field orientations [37], so as to calculate the filament dc susceptibility, $\chi_{\rm fil}$ (Fig. 2). When H//wire, the transitions are rather broad [Figs. 2(c) and 2(d)] and the low-temperature $\chi_{\rm fil}$ ranges from ~ -1 to ~ -1.4 for the 1-mm wires, and between ~ -0.8 and ~ -1.3 for the 1.2-mm wires. In contrast, when $H\perp$wire, the transitions are rather sharp but $\chi_{\rm fil}$ at low temperature tends to ~ -1.4 in all samples.

These results lead to two important observations: the first being that $\chi_{\rm fil}$ assumes unphysical values ($\chi_{\rm fil} < -1$); the second being that there is an obvious sample-to-sample difference for H//wire, but only limited variation (mostly near T_c) for $H\perp$wire. These findings can be understood as follows: in an ideal case [H//wire in Fig. 2(a)], the supercurrent should only screen the filament volumes and $\chi_{\rm fil}$ should reach at most the minimal value of -1 at low temperature. However, because of the bridged filaments, the samples can be schematized as shown in Fig. 2b (H//wire): some of the bridges have supercurrent capability, leading to screening loops including many filaments, meaning that there is a significant volume of nonsuperconducting phase (Ag) that is also shielded, causing unphysical $\chi_{\rm fil}$ values when the filament size is initially assumed. Moreover, in this configuration, when the cooling rate decreases from 5 to 1 °C/h, the absolute value of $\chi_{\rm fil}$ progressively increases, implying that there are wider supercurrent loops screening a larger nonsuperconducting volume at slower cooling rates. This trend can clearly be correlated to the microstructural variations observed in Fig. 1, where greater bridging is observed in the slower-cooled wire with longer $t_{\rm melt}$.

Although the explanation for the excess shielding is similar for the $H\perp$wire [Fig. 2(e)], the small sample-to-sample variation of $\chi_{\rm fil}$ at low temperature means that all wires have a similar shielded volume. This is likely related to the smaller λ_{ab} (in anisotropic materials $\gamma = \xi_{ab}/\xi_c = \lambda_c/\lambda_{ab} > 1$), which dominates in this configuration, making most bridges effective in connecting the filaments: this generates very large loops with small sample-to-sample variation. On the contrary, for H//wire, the field is almost parallel to the Bi-2212 *ab* planes and to the dominant *ab*-plane GBs: with the larger λ_c affecting many filament bridges and making easier GB field penetration, the supercurrent capability of the bridges is likely reduced, leading to suppressed shielding. The large anisotropy of the penetration depths, $\lambda_{ab} \ll \lambda_c$, is what causes the large variation in the transition broadening between the perpendicular and parallel configurations.

What still needs an explanation is why $\chi_{\rm fil}$ reaches the unexpected large shielding of $\chi_{\rm fil} \sim -1.4$ ($H\perp$wire): in other words, what is the actual shielded volume and the characteristic size of the shielding? Considering the wire design, we could presume that the actual shielded volume is related to the filament bundles, constituted by 85 filaments each. To verify this hypothesis, we assumed that the bridging operates at the whole bundle level, with the wire behaving like 18 cylindrical first-stack bundles. This enabled us to back calculate the shielded diameters, $d_{\rm shielding}$, which gave values of 159–163 μm and 181–189 μm for the 1- and 1.2-mm wires, respectively. These values are indeed very close to the densified equivalent diameters of the bundles estimated from the cross sections (163 and 195 μm).

Summarizing, the dc characterization reveals that all 85 filaments within a bundle are effectively bridged for $H\perp$wire axis, regardless of the actual wire microstructure. Therefore, the relevant size for magnetic characterizations of the superconducting component of the wire in this configuration is that of the bundle, not the filament. Despite not being relevant for magnet application, measuring with H parallel to the wire axis is a useful and rapid technique to estimate how changing processing parameters affect the extent of filament bridging: it could for instance be used to evaluate the effect of any relevant HT variable.

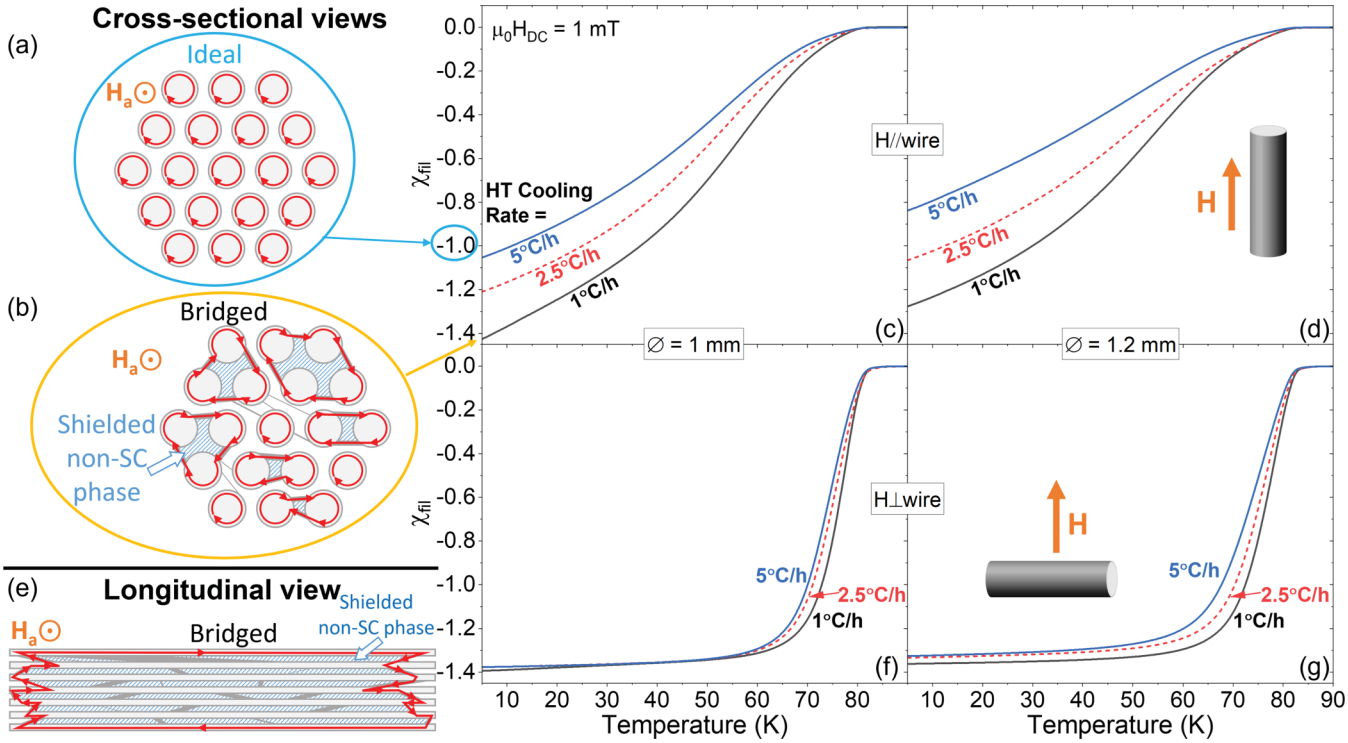

FIG. 2. (a), (b) Two-dimensional schematics (not to scale) of shielding in a multifilamentary Bi-2212 conductor, for H//wire, in the ideal (a) and the bridged (b) cases showing filaments (circles), bridges (straight lines joining the filaments), and the shielding currents (paths with arrows); in (b), striped regions between filaments represent a nonsuperconducting phase shielded by supercurrent percolating through the bridges. These simplified sketches explain how $|\chi_{fil}|$ can exceed 1. (c), (d) Temperature dependence of χ, estimated from the filament sizes, for magnetic field applied along the wire axis showing an apparently unphysical trend (see text for explanation); data for the 1- and 1.2-mm-diameter wires heat treated with different cooling rates are shown. (e) 2D schematic (not to scale, similarly to (b)) of shielding in a bridged multifilamentary Bi-2212 conductor for $H\perp$wire. (f)-(g) Data as in panels (c)-(d), but for magnetic field perpendicular to the wires.

B. ac susceptibility: $\mu_0 H_{dc} = 0$ T

ac susceptibility characterization was performed to evaluate the first harmonic χ_1. Because of the results obtained by the dc characterization, χ_1 was calculated using the equations suggested by Goldfarb *et al.* [21] and the demagnetization factor for cylinders with a diameter $d_{\text{shielding}}$ calculated from the dc magnetization. Because of the irregular geometry of the coupled-filament microstructure, this is clearly an approximation; however, despite the exact shape not being known (nor its variability from bundle to bundle), the data will show that this approximation is reasonable. To distinguish the dc measurements of Fig. 2 from the following ac figures, the ac characterizations are marked with $\chi_{1,\text{bundle}}$, although for simplicity we will refer to it in the text simply as χ_1.

1. Superconducting and normal phases

The first step was to explore the frequency, f, and H_{ac} dependences of χ_1 to identify the superconducting and normal features in the ac data. Figure 3 reports the real (lower) and imaginary (upper) parts, χ_1' and χ_1'', of the ac susceptibility for $\mu_0 H_{dc} = 0$ T. The obvious χ_1'' peaks at ~73−80 K correspond well with the sharp diamagnetic signal (χ_1') that reveals the rapid development of the superconducting phase. However, a second peak becomes visible at much lower temperature [e.g., below 10 K at 73 Hz in Fig. 3(b)] that has no H_{ac} dependence [Fig. 3(b)], but also obviously shifts toward higher temperature with increasing frequency [Fig. 3(a)] and becomes more visible. This behavior is consistent with losses generated in a normal phase by the eddy current [whose skin depth is determined by $\delta = (2\rho/\mu_0\omega)^{1/2}$ with ρ being the resistivity and $\omega = 2\pi f$] [20] with the normal phase being the Ag matrix surrounding the filaments. This identification is confirmed by the almost identical overall features found in monofilamentary 2223 tape by Savvides and Muller [33], where the issue was also theoretically investigated. The effect of Ag on ac susceptibility was also investigated in Bi-2212 conductors [35,36]: it was observed that the Ag contribution was more pronounced when the conductors were measured for H//wire and the use of low frequency was recommended to more easily evaluate the superconducting phase, in particular in this configuration.

Figure 4 shows the Cole-Cole plots (χ_1'' versus χ_1') for some of the data in Fig. 3. This reveals the typical bell shape associated with the superconducting behavior, where χ_1'' is expected to go to 0 as $\chi_1' \to -1$, if the normal state contribution at low χ_1' is neglected. The Cole-Cole plots indeed help identify the normal contribution, which, in fact, shifts the curves upward and generates obvious deviations at low temperatures where the normal-state conductivity becomes large.

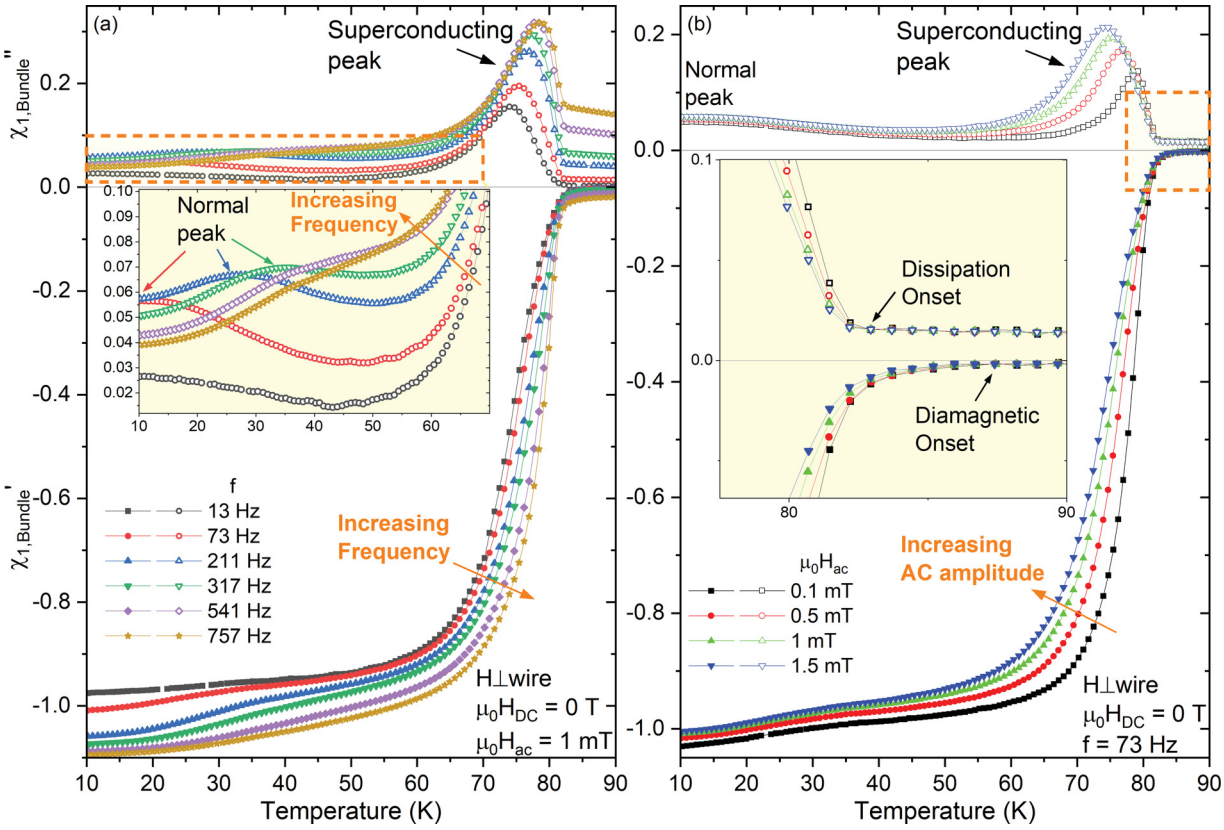

FIG. 3. Two-dimensional temperature dependence of the ac susceptibility of a Bi-2212 wire (5 °C/h) for $H\perp$wire, evaluated using the bundle- rather than filament scale (see text), measured at different (a) frequencies and (b) ac amplitudes at zero-dc field. The real, $\chi'_{1,\text{bundle}}$, and imaginary, $\chi_{1,\text{bundle}}{}''$, parts are plotted. The inset in (a) highlights the rapid shift toward high temperature of the normal eddy-current peak with increasing frequency. The inset in (b) highlights the difference between the dissipative and the diamagnetic onsets.

2. *Superconducting properties*

The $\mu_0 H_{dc} = 0$ T data, described above, reveal no splitting of the dissipative superconducting peaks and no obvious double-diamagnetic transitions. However, as emphasized in the inset of Fig. 3(b), the dissipation and diamagnetic onsets do not coincide. The diamagnetic signal has a high-temperature onset, which however involves only a few percent of the transition; the major diamagnetic transition then occurs in correspondence with the dissipation peak. This trend indeed suggests the presence of two distinct supercurrent contributions. The lack of a high-temperature dissipation peak χ_1'' at zero-dc field is likely due to our sensitivity limit. In fact, for comparison, we note that Goldfarb's results on polycrystal YBCO had 70% of the high-temperature diamagnetic signal caused by intragrain current but the corresponding dissipation peak was only 1/10 of the low-temperature intergrain peak [26].

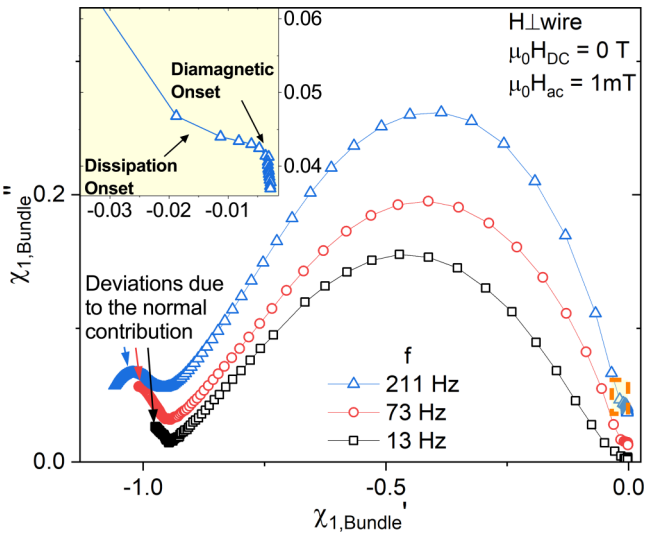

FIG. 4. Cole-Cole plots for some of the data in Fig. 3, evaluated on the bundle scale. The inset highlights the region near the onset of superconductivity pointing out the different onsets.

Comparing the two wires (not shown), we found no difference in the dissipation and diamagnetic onset values: in both cases, they are at ~82.9 and 87.4 K. Just as in the dc characterizations, the high-J_c sample (1 °C/h) has a sharper transition.

Summarizing the frequency and amplitude dependences of the ac susceptibility at zero-dc field, we were able to distinguish features related to the superconducting phase from those of the Ag normal matrix. Moreover, the observation that $\chi_1'' \to 0$ for $\chi_1' \to -1$ at low frequency confirms that the cylindrical bundle approximation is indeed correct. Differently from previous HTS characterizations, no obvious features induced by multiple supercurrent contributions are observed. However, the difference in the diamagnetic and

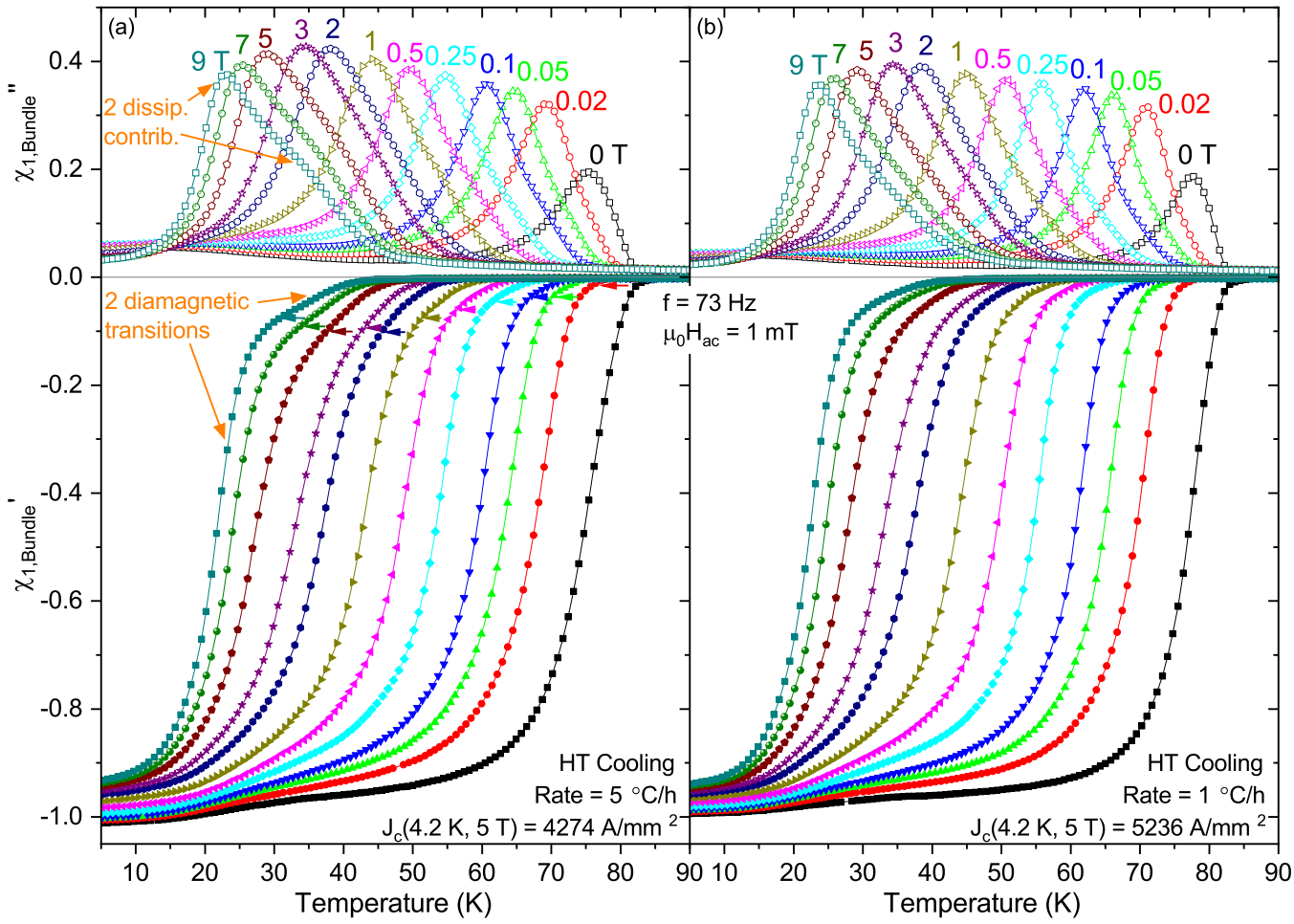

FIG. 5. Temperature dependence of the ac susceptibility (evaluated on the bundle scale) of the (a) low-J_c and (b) high-J_c Bi-2212 1.2-mm wires, measured with different dc fields for $H\perp$wire. In (a) the two diamagnetic transitions and two dissipation contributions are highlighted for the 9-T data; the small arrows next to the χ_1' curves indicate the approximate locations of the intergrain onset. The higher-temperature diamagnetic transition and dissipation contribution are slightly less evident in the high-J_c wire.

dissipative T_c onsets suggests the possibility of a split superconducting transition.

C. ac susceptibility: $\mu_0 H_{dc}$ up to 9 T

As explained above, to limit the influence of the normal matrix contribution on the analysis of the superconducting properties, we investigated the H_{dc} dependence of the ac susceptibility at relatively low frequency ($\leqslant 211$ Hz). In fact, in these conditions and for $H\perp$wire, the superconducting and normal peaks are still clearly separate at low H_{dc}; with increasing H_{dc}, the Ag magnetoresistance sharply increases, progressively suppressing and moving the normal peak toward lower temperature, until its effect becomes negligible (behind a linear background) on the superconducting signal. The suppressed Ag effect with increasing field is confirmed by the low-temperature trend of χ_1'' (see Fig. 5): in fact, $\chi_1''(5\text{ K})$ clearly decreases at field larger than 0.25 T. Also in this case, we used the Cole-Cole plots to easily identify the range of data affected by the normal Ag contributions to the dissipation, and to exclude them from the peak analysis described below. Similarly to Fig. 4, also for the in-field data (not shown) the Ag contribution appears in the Cole-Cole plot only at very low χ_1'' (corresponding to very low temperature) and it rapidly disappears with increasing field.

1. Intergrain and intragrain contributions

Figure 5 reports the ac susceptibility obtained with $\mu_0 H_{dc}$ up to 9 T for the low- and high-J_c wires. Applying a rather small dc field, 0.02 T, the dissipation of the superconducting phase almost doubles with respect to $\mu_0 H_{dc} = 0$ T, suggesting that a second source of dissipation becomes suddenly effective. With increasing H_{dc}, the curves clearly develop two superconducting diamagnetic transitions in χ_1', with two corresponding dissipation contributions in χ_1'' [see marked features for the 9-T data in Fig. 5(a)]. As is done for other HTS materials, we interpret these two contributions as being determined by intergrain and intragrain currents at the lower and higher temperatures, respectively. It is important to notice that the intergrain current still operates at the bundle level, as χ_1' calculated with the bundle sizes roughly tend to -1 even at high H_{dc}. The following analysis will justify the interpretation that the higher-temperature dissipative contribution is indeed intragrain.

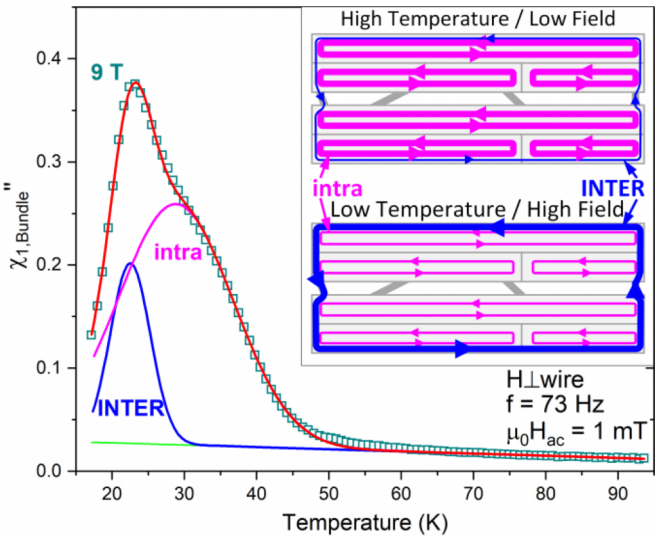

FIG. 6. Temperature dependence of χ_1'' (evaluated on the bundle scale) for a Bi-2212 wire (5 °C/h) measured at $\mu_0 H_{dc} = 9$ T, fitted with a 2-Gaussian curve. The insets represent the changes in the intra-/intergrain relative currents, induced into the grains (sketched as small rectangles) and into the bundles (sketched as bridged filaments), as field and temperature are changed.

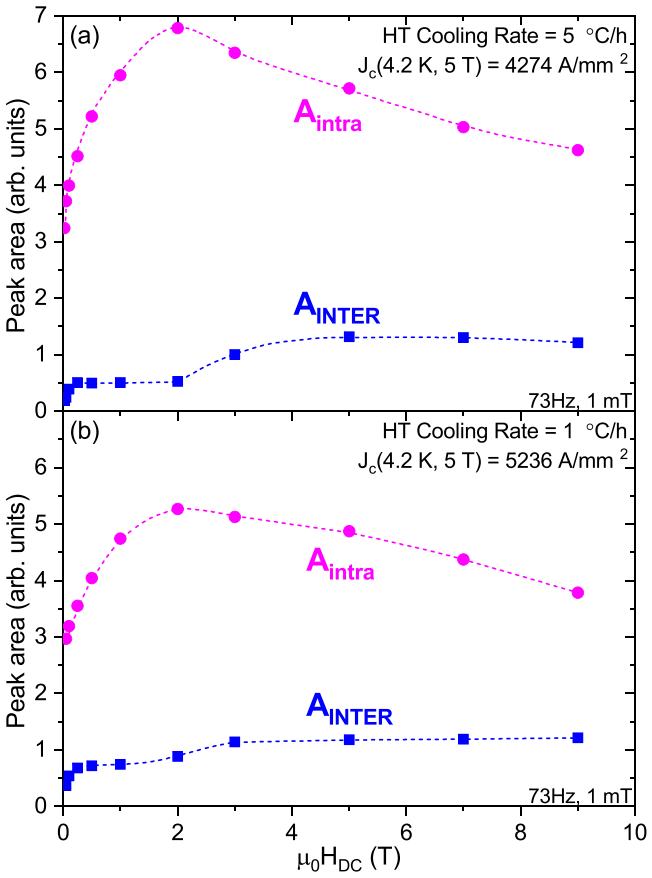

FIG. 7. Peak areas of the intra- and intergrain contributions as a function of H_{dc} for the (a) low- and (b) high-J_c 1.2-mm Bi-2212 wires.

Although both wires show the same two-contribution feature, the intragrain (higher-temperature) contribution is more pronounced in the low-J_c wire [Fig. 5(a)], indicating that a larger fraction of the induced current is intragrain limited, a sign of connectivity issue.

To better quantify the sample differences and their changes with H_{dc}, the χ_1'' data were analyzed with a double-Gaussian fit above a linear background to estimate the peak positions and their sizes. As shown in Fig. 6, the two peaks clearly differ in widths justifying the initial inter-/intragrain interpretation. The reason is that the intragrain component is determined by current inside randomly oriented grains, which have different $J_c(H)$ dependences due to their varying orientation (H with respect to c axis) and so they generate a broad peak. The intergrain component is instead determined by current percolating through biaxially oriented grains and GBs, and they are typically limited by a relatively low-J_c path (e.g., J_c of the grains with $H//c$) limiting the peak broadening. The higher-temperature peak cannot be attributed to current at the filament level: since the c axis is rotating along the filament length, the filament current would be limited by any low-J_c path as well, and so would have the same narrow peak found for the intergrain bundle-level contribution.

The change in inter- and intragrain peak areas (A_{inter} and A_{intra}) with increasing H_{dc} is reported in Fig. 7 and it shows a change of trend at intermediate field and temperature (because of the peak shifting at low temperature with increasing H_{dc}, field- and temperature dependences are anticorrelated). In fact, with increasing H_{dc} up to ∼1–2 T, the intragrain dissipation sharply increases, whereas the intergrain contribution plateaus after an initial increase. At higher H_{dc} (up to 9 T), the intragrain contribution gradually decreases, whereas the intergrain dissipation first increases and then plateaus again. The general trend is substantially the same in both samples: the only difference is that in the high-J_c wire [Fig. 7(b)] A_{inter}, after the first plateau, appears to increase at slightly lower field than the low-J_c wire (i.e., between 1 and 2 T, instead of just above 2 T of the low-J_c case). We verified the corresponding temperature of these features: in both wires the maximum of A_{intra} is at about 40 K, whereas A_{inter} increases from the first to the second plateau at a temperature between 38 and 45 K in the high-J_c sample and only at 33–37 K in the low J_c wire.

This regime change suggests that up to ∼1–2 T there is an increasing fraction of current confined within the grains, but at high H_{dc} (i.e., low temperature) the intergrain contribution grows causing a decrease in the intragrain dissipation; this scenario is schematically illustrated in the inset of Fig. 6 and it is further confirmed by the general trend of χ_1' in Fig. 5. In fact, the double transition is typically interpreted as a measure of the volume of the sample shielded by intragrain and intergrain currents (although they partially overlap here). In Fig. 5(a) the approximative locations of the intergrain χ_1' onsets are marked by small arrows next to the curves (intergrain onsets are estimated as $T_{p,\text{inter}} + 3\sigma_{\text{inter}}$ as determined from the χ_1'' double-Gaussian fits, where $T_{p,\text{inter}}$ and σ_{inter} are the peak position and standard deviation of the lower-temperature Gaussian): they show that the intragrain contribution (above the arrows) increases up to 2 T, and then it slowly decreases. This regime change could be caused by possibly two

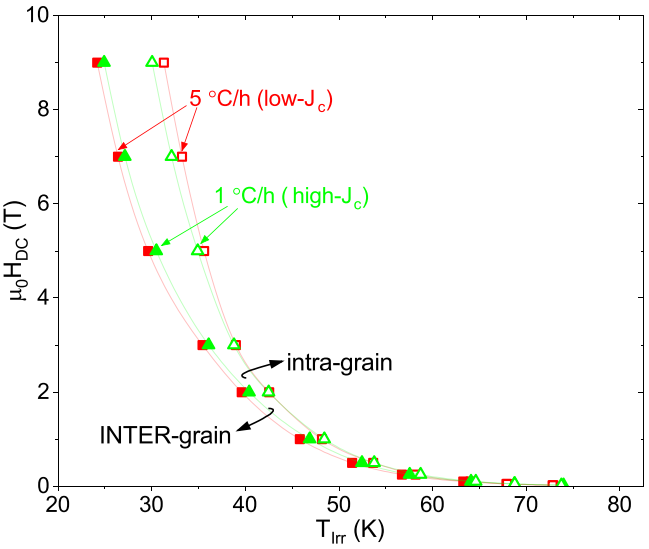

FIG. 8. Irreversibility lines of the low- and high-J_c Bi-2212 wires estimated for both the intragrain and the intergrain contribution to the dissipation.

low-temperature effects: the appearance of an additional pinning mechanism (e.g., intragrain point pinning) and/or an improvement of the grain-boundary transparency.

Summarizing, with increasing H_{dc} and shifting toward low temperature of the transitions, two distinctive superconducting features become apparent in χ_1' and χ_1'': they can be correlated to the intergrain and intragrain currents at the lowest and highest temperatures, respectively. Both χ_1' trend and χ_1'' analysis reveal a change of regime at ∼1–2 T, when the contribution from the intragrain current starts decreasing in favor of the intergrain current. The increase of the intergrain current occurs at lower temperature in the low-J_c wire with respect to the high-J_c wire, indicating weaker pinning and/or inferior GB transparency in the low-J_c wire.

2. H_{ac} dependence and irreversibility fields

Because of the presence of the inter- and intragrain contributions, two irreversibility lines can be determined for each wire. This can be done by investigating the positions of the χ_1'' peaks as a function of amplitude H_{ac} (varied from 0.1 to 1.5 mT) [38,39]. Since by definition $J_c = 0$ at the irreversibility line and considering that $J_c \propto H_{ac}$, for each H_{dc}, $T_{\mathrm{irr,intra}}$, and $T_{\mathrm{irr,inter}}$ are determined as the limit of peak positions for H_{ac} tending to zero [28]. As expected, the peaks slightly shift toward higher temperature with decreasing H_{ac} and the obtained irreversibility lines are reported in Fig. 8.

We observed that $T_{\mathrm{irr,intra}}$ is clearly higher than $T_{\mathrm{irr,inter}}$ with a difference at 9 T of 5.2 and 7.1 K for the high- and low-J_c wires, respectively (see Table II). The $T_{\mathrm{irr,inter}}$ difference between the two samples is rather small, but $T_{\mathrm{irr,inter}}$ is always better in the high-J_c wire. This is expected considering that transport J_c is typically limited by the intergrain performance. A more marked difference is instead observed in $T_{\mathrm{irr,intra}}$, which, on the contrary, is better in the low-J_c wire. The peak broadening, estimated as the $T_{\mathrm{irr}} \pm 3\sigma$ at 9 T from the double-Gaussian fits, is also noticeably different between

TABLE II. Comparison at 9 T of the inter- and intragrain irreversibility field and their distributions for two 2212 wires.

HT cooling rate °C/h	$T_{\mathrm{irr,inter}}$ (9 T) K	$T_{\mathrm{irr,intra}}$ (9 T) K	$T_{\mathrm{irr,inter}} \pm 3\sigma_{\mathrm{inter}}$ (9 T) K	$T_{\mathrm{iir,intra}} \pm 3s_{\mathrm{intra}}$ (9 T) K
1	24.9	30.1	16.2–33.7	7.7–52.5
5	24.2	31.3	14.9–33.5	11.4–51.2

the two samples, particularly for the intragrain contribution (Table II): for the high-J_c wire (1 °C/h) $T_{\mathrm{irr,intra}} \pm 3\sigma$ ranges from 7.7 to 52.5 K, whereas for the low-J_c wire (5 °C/h) it varies between 11.4 and 51.2 K. So, the high-J_c wire has a wider range of intragrain T_{irr}. This is likely caused by a difference in the anisotropy, possibly caused by variation in atomic disorder or vacancy density; however, we cannot exclude an indirect effect due to the microstructure. In fact, the intragrain properties are determined by the current induced into the grains on a scale of λ: so, the ac signal could be less sensitive measuring a small-grain wire producing a narrow intragrain peak that, however, is not related to the intrinsic properties of the 2212 phase. Grain size and biaxial texturing could also affect the intergrain properties: in fact, the grain size affects the contact surface of adjacent grains and thus the grain-to-grain supercurrent capability, whereas a large grain misorientation would intrinsically suppress the supercurrent across grain boundaries. Interestingly, the sample differences in $T_{\mathrm{irr,inter}} \pm 3\sigma$ (9 T) are rather small and the high-J_c wire has a narrower and higher temperature range, suggesting subtle differences caused by the microstructure.

Summarizing, we found a clear separation between the intragrain and intergrain irreversibility lines with the latter being at lower temperature. As expected, the high-J_c sample has a better intergrain irreversible behavior, but the opposite trend is found for the intragrain T_{irr}, which also has a wider range in the high-J_c wire. This wide range of $T_{\mathrm{irr,intra}}$ clearly does not have a direct impact on $T_{\mathrm{irr,inter}}$ and on the overall intergrain performance. Extensive microstructural characterization, which is outside the scope of this paper, might clarify whether details of the grain morphology and variations of grain size and biaxial texture could cause the unexpected intragrain irreversibility behavior.

3. f dependence and pinning energies

The frequency dependence provides information about the pinning performance. Figure 9 shows an example at 9 T revealing that the intergrain contribution is only marginally affected by the frequency change: in fact, the main χ_1'' peak is not strongly shifted in temperature. On the contrary, the intragrain contribution significantly changes both in amplitude and position. Since $f/f_0 = \exp(-U_0/k_B T_p)$ (with U_0 being the pinning energy, f_0 the characteristic frequency, and T_p the peak position) [22], U_0 can be estimated from the slope of the Arrhenius plots, as shown in the insets of Fig. 10, and the resulting intergrain and intragrain U_0 are plotted as a function of H_{dc} in the main panels. $U_{0,\mathrm{inter}}$ roughly follows a power law [Fig. 10(a)], whereas $U_{0,\mathrm{intra}}$ is enhanced at field above ∼1–2 T with respect to an initial power-law trend [Fig. 10(b)].

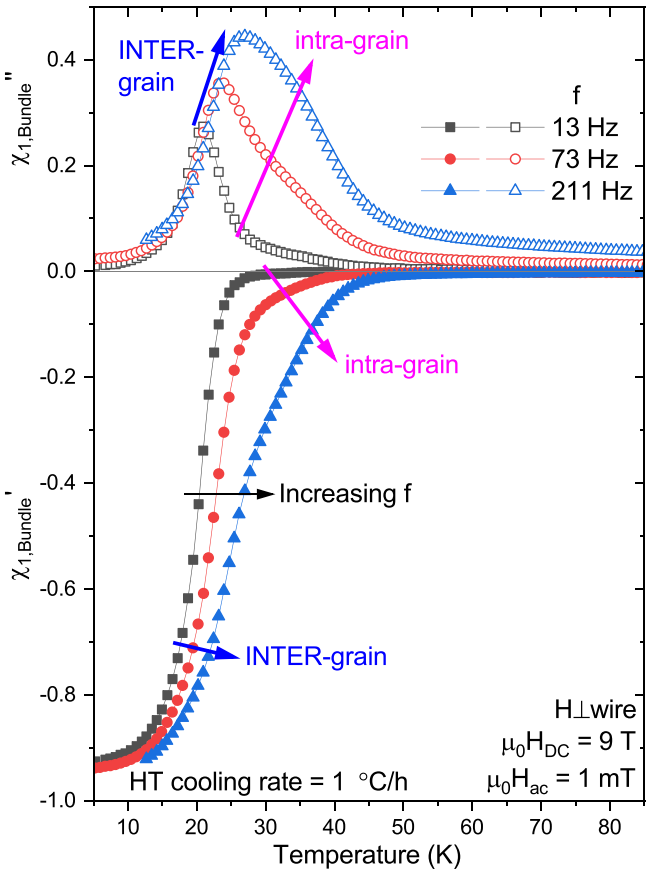

FIG. 9. Temperature dependence of the ac susceptibility (evaluated on the bundle scale) of a Bi-2212 wire, measured at different frequencies, showing the weak variation on the features associated with the intergrain contribution and a stronger change in the intragrain properties.

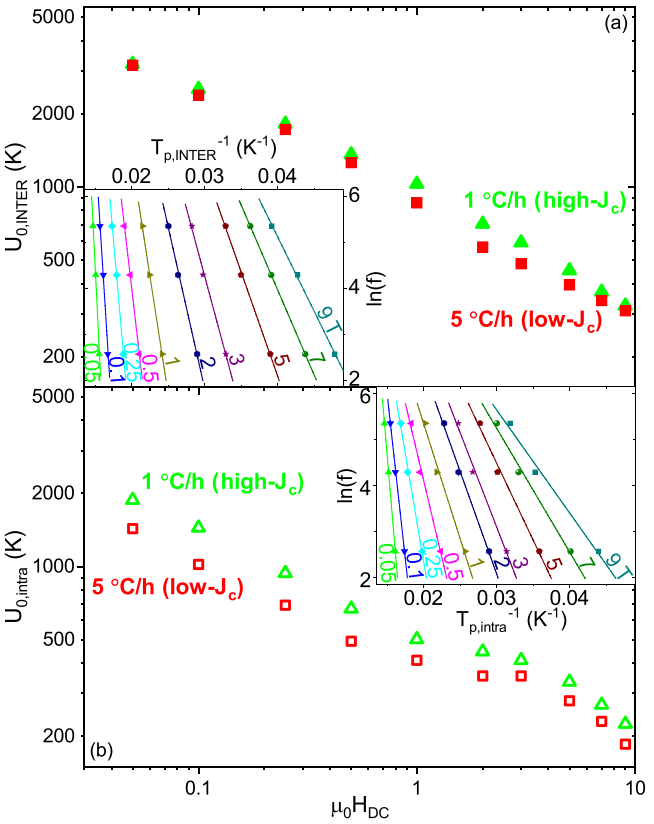

FIG. 10. dc field dependence of the pinning energies, U_0, for the (a) inter- and (b) intragrain contributions of the low- and high-J_c 2212 wires, estimated from the $\mu_0 H_{ac} = 1$ mT data. In the insets, the inter- and intragrain Arrhenius plots of a Bi-2212 wire.

Note that this is the same field range at which the change of regime was observed in Fig. 7.

Interestingly, the intergrain pinning is always stronger than the intragrain one. Although this might appear surprising, the intragrain pinning is likely weak until the point pinning starts becoming effective at low T (as demonstrated by the $U_{0,\mathrm{intra}}$ enhancement above ∼1–2 T) and $U_{0,\mathrm{inter}}$ is presumably affected by both the intragrain and the intergrain pinning. The intragrain pinning could also be the cause of the minor deviation from the power law of the $U_{0,\mathrm{inter}}$ versus field trend. As expected, the high-J_c wire has larger pinning energies than the low-J_c wire for both contributions.

It is important to notice the strong changes in χ_1' with increasing frequency (Fig. 9). In fact, the intragrain contribution to the diamagnetic signal increases from only a few percent at 13 Hz to ∼30% at 211 Hz. This means that there is an increasingly large fraction of current that is limited to the grain and does not contribute to the overall diamagnetic signal. This means that the weak intragrain pinning is actually key to achieve a significant intergrain current.

Summarizing, the evaluation of the intergrain and intragrain pinning energies reveals that the intragrain is weaker in these samples, although some enhancement is observed at field above 1–2 T. Moreover, the reduction of the intergrain diamagnetic contribution with increasing frequency is caused by the activation of the vortices weakly pinned on intragrain defects, emphasizing the essential role they play in the intergrain performances.

IV. CONCLUSION

In this paper, we demonstrated the value of performing detailed magnetic characterizations of state-of-the-art overpressure heat-treated Bi-2212 wires. At small dc fields, we found that the magnetically induced currents flow at the whole-bundle level when H is perpendicular to the wire, independent of the visual estimation of filament bonding or bridging. Using low-frequency ac susceptibility (which suppressed Ag-matrix eddy current) with increasing dc field, we were able to identify two superconducting current contributions. From the shielded volume and the different widths of the dissipative peaks, we established that the intergrain contribution at the bundle level dominates at lower temperatures, whereas the dominant high-temperature contribution is at the intragrain level. We found a clear separation of ∼5–7 K at 9 T between the intragrain and intergrain irreversibility lines with only small sample-to-sample differences. The highest-J_c sample has a higher intergrain irreversibility line but also a broader range of intragrain T_{irr}, which could be determined by differences in anisotropy or variable microstructural features, which are under further characterization. Both the amplitude

of the intragrain dissipation and the intragrain vortex pinning energy indicate that additional intragrain pinning starts to be effective below 35–40 K. Strikingly, this leads also to an increase of the intergrain current. Because the intragrain current density defines the upper limit to the current that can cross the grain boundaries, it also plays an essential role in determining the overall properties of Bi-2212 wires.

In general, this paper shows that ac susceptibility is a valuable tool for understanding the complexity of current flow in today's best-performing Bi-2212 wires. We plan to carry out further studies of differently prepared and processed wires with both higher and lower J_c to probe the performance limits of Bi-2212 wires.

ACKNOWLEDGMENTS

This work was supported by the U.S. DOE Office of High Energy Physics under Grant No. DE-SC0010421, was performed at the NHMFL, which is supported by the NSF under Award No. DMR-1644779 and by the State of Florida, and was performed under the purview of the U.S. Magnet Development Program (MDP).

[1] D. C. Larbalestier, J. Jiang, U. P. Trociewitz, F. Kametani, C. Scheuerlein, M. Dalban-Canassy, M. Matras, P. Chen, N. C. Craig, P. J. Lee, and E. E. Hellstrom, Isotropic round-wire multifilament cuprate superconductor for generation of magnetic fields above 30 T, Nat. Mater. **13**, 375 (2014).

[2] P. Chen, U. P. Trociewitz, J. Lu, E. S. Bosque, J. Jiang, E. E. Hellstrom, and D. C. Larbalestier, Experimental study of potential heat treatment issues of large Bi-2212 coils, IEEE Trans. Appl. Supercond. **27**, 4601405 (2017).

[3] K. Zhang, H. Higley, L. Ye, S. Gourlay, S. Prestemon, T. Shen, E. Bosque, C. English, J. Jiang, Y. Kim, J. Lu, U. Trociewitz, E. Hellstrom, and D. Larbalestier, Tripled critical current in racetrack coils made of Bi-2212 Rutherford cables with overpressure processing and leakage control, Supercond. Sci. Technol. **31**, 105009 (2018).

[4] T. Shen, E. Bosque, D. Davis, J. Jiang, M. White, K. Zhang, H. Higley, M. Turqueti, Y. Huang, H. Miao, U. Trociewitz, E. Hellstrom, J. Parrell, A. Hunt, S. Gourlay, S. Prestemon, and D. Larbalestier, Stable, predictable and training-free operation of superconducting Bi-2212 Rutherford cable racetrack coils at the wire current density of 1000 A/mm^2, Sci. Rep. **9**, 10170 (2019).

[5] L. Garcia Fajardo, T. Shen, X. Wang, C. Myers, D. Arbelaez, E. Bosque, L. Brouwer, S. Caspi, L. English, S. Gourlay, A. Hafalia, M. Martchevskii, I. Pong, and S. Prestemon, First demonstration of high current canted-cosine-theta coils with Bi-2212 Rutherford cables, Supercond. Sci. Technol. **34**, 024001 (2021).

[6] F. Kametani, J. Jiang, M. Matras, D. Abraimov, E. E. Hellstrom, and D. C. Larbalestier, Comparison of growth texture in round Bi2212 and flat Bi2223 wires and its relation to high critical current density development, Sci. Rep. **5**, 8285 (2015).

[7] T. Shen, J. Jiang, F. Kametani, U. P. Trociewitz, D. C. Larbalestier, J. Schwartz, and E. E. Hellstrom, Filament to filament bridging and its influence on developing high critical current density in multifilamentary $Bi_2Sr_2CaCuO_x$ round wires, Supercond. Sci. Technol. **23**, 025009 (2010).

[8] F. Kametani, T. Shen, J. Jiang, C. Scheuerlein, A. Malagoli, M. Di Michiel, Y. Huang, H. Miao, J. A. Parrell, E. E. Hellstrom, and D. C. Larbalestier, Bubble formation within filaments of melt-processed Bi2212 wires and its strongly negative effect on the critical current density, Supercond. Sci. Technol. **24**, 075009 (2011).

[9] C. Scheuerlein, M. Di Michiel, M. Scheel, J. Jiang, F. Kametani, A. Malagoli, E. E. Hellstrom, and D. C. Larbalestier, Void and phase evolution during the processing of Bi-2212 superconducting wires monitored by combined fast synchrotron micro-tomography and x-ray diffraction, Supercond. Sci. Technol. **24**, 115004 (2011).

[10] J. Jiang, W. L. Starch, M. Hannion, F. Kametani, U. P. Trociewitz, E. E. Hellstrom, and D. C. Larbalestier, Doubled critical current density in Bi-2212 round wires by reduction of the residual bubble density, Supercond. Sci. Technol. **24**, 082001 (2011).

[11] J. Jiang, H. Miao, Y. Huang, S. Hong, J. A. Parrell, C. Scheuerlein, M. Di Michiel, A. K. Ghosh, U. P. Trociewitz, E. E. Hellstrom, and D. C. Larbalestier, Reduction of gas bubbles and improved critical current density in Bi-2212 round wire by swaging, IEEE Trans. Appl. Supercond. **23**, 6400206 (2013).

[12] A. Malagoli, C. Bernini, V. Braccini, G. Romano, M. Putti, X. Chaud, and F. Debray, Large critical current density improvement in Bi-2212 wires through the groove-rolling process, Supercond. Sci. Technol. **26**, 045004 (2013).

[13] A. Malagoli, V. Braccini, M. Vignolo, X. Chaud, and M. Putti, Groove-Rolling as an alternative process to fabricate Bi-2212 wires for practical applications, Supercond. Sci. Technol. **27**, 055022 (2014).

[14] C. Scheuerlein, A. Rack, K. Schladitz, and L. Huwig, Synchrotron microtomography investigation of the filament microstructure in differently processed Bi-2212 wires, IEEE Trans. Appl. Supercond. **27**, 6400205 (2017).

[15] J. Jiang, A. Francis, R. Alicea, M. Matras, F. Kametani, U. P. Trociewitz, E. E. Hellstrom, and D. C. Larbalestier, Effects of filament size on critical current density in overpressure processed Bi-2212 round wire, IEEE Trans. Appl. Supercond. **27**, 6400104 (2017).

[16] J. Jiang, S. I. Hossain, T. A. Oloye, Y. Oz, S. Barua, J. Cooper, E. Miller, Y. Huang, J. A. Parrell, F. Kametani, U. P. Trociewitz, E. E. Hellstrom, and D. C. Larbalestier, Effects of wire diameter and filament size on the processing window of Bi-2212 round wire, IEEE Trans. Appl. Supercond. **31**, 6400206 (2021).

[17] Y. Oz, D. Davis, J. Jiang, E. E. Hellstrom, and D. C. Larbalestier, Influence of twist pitch on hysteretic losses and transport J_c in overpressure processed high J_cBi-2212 round wires, Supercond. Sci. Technol. **35**, 064004 (2022).

[18] A. Angrisani Armenio, A. Leveratto, G. de Marzi, A. Traverso, C. Bernini, G. Celentano, and A. Malagoli, Investigation of transport mechanisms induced by filament-coupling bridges-network in Bi-2212 wires, Supercond. Sci. Technol. **35**, 035002 (2022).

[19] M. D. Brown, J. Jiang, C. Tarantini, D. Abraimov, G. Bradford, J. Jaroszynski, E. E. Hellstrom, and D. C. Larbalestier,

Prediction of the $J_C(B)$ behavior of Bi-2212 wires at high field, IEEE Trans. Appl. Supercond. **29**, 6400504 (2019).

[20] F. Gömöry, Characterization of high-temperature superconductors by AC susceptibility measurements, Supercond. Sci. Technol. **10**, 523 (1997).

[21] R. B. Goldfarb, M. Lelentan, and C. A. Thompson, *Alternating-Field Susceptometry and Magnetic Susceptibility of Superconductors, in Magnetic Susceptibility of Superconductors and Other Spin Systems*, edited by T. L. Francavilla, R. A. Hein, and D. H. Liebenberg (Plenum Press, New York, 1991), p. 49.

[22] M. Nikolo and R. B. Goldfarb, Flux creep and activation energies at the grain boundaries of Y-Ba-Cu-O superconductors, Phys. Rev. B **39**, 6615 (1989).

[23] D.-X. Chen, J. Nogues, and K. V. Rao, A.c. Susceptibility and intergranular critical current density of high Tc superconductors, Cryogenics **29**, 800 (1989).

[24] M. Polichetti, M. G. Adesso, D. Zola, J. Luo, G. F. Chen, Z. Li, N. L. Wang, C. Noce, and S. Pace, Granularity and vortex dynamics in $LaFeAsO_{0.92}F_{0.08}$ probed by harmonics of the ac magnetic susceptibility, Phys. Rev. B **78**, 224523 (2008).

[25] D. Mancusi, M. Polichetti, M. R. Cimberle, and S. Pace, Influence of the interaction between the Inter- and Intragranular magnetic responses in the analysis of the ac susceptibility of a granular $FeSe_{0.5}Te_{0.5}$ Superconductor, Supercond. Sci. Technol. **28**, 095017 (2015).

[26] R. B. Goldfarb, A. F. Clark, A. I. Braginski, and A. J. Panson, Evidence for two superconducting components in oxygen-annealed single-phase Y-Ba-Cu-O, Cryogenics **27**, 475 (1987).

[27] M. Forsthuber, F. Ludwig, and G. Hilscher, Size dependence of the AC susceptibility and critical current densities of ceramic high-T_c superconductors, Physica C **177**, 401 (1991).

[28] F. Gömöry and S. Takács, Irreversibility line and non-linearity in the AC response caused by flux pinning in high-Tc superconductors, Physica C **217**, 297 (1993).

[29] A. Wang and C. Petrovic, Vortex pinning and irreversibility fields in $Fe\,S_{1-x}Se_x (x = 0,\ 0.06)$, Appl. Phys. Lett. **110**, 232601 (2017).

[30] S. X. Dou, J. Horvat, X. L. Wang, M. Ionescu, H. K. Liu, I. Kusevic, and E. Babic, Comparative studies on single crystals and superconducting Bi-(Pb)-Sr-Ca-Cu-O tapes, IEEE Trans. Appl. Supercond. **7**, 2219 (1997).

[31] J.-F. Fagnard, P. Vanderbemden, R. Cloots, and M. Ausloos, Anisotropic AC behavior of multifilamentary Bi-2223/Ag tapes, IEEE Trans. Appl. Supercond. **13**, 2976 (2003).

[32] A. Gencer, S. Nezir, M. Altunbas, and A. Aydinuraz, AC susceptibility study of BiPbSrCaCuO(2223) superconductors, Supercond. Sci. Technol. **9**, 467 (1996).

[33] N. Savvides and K.-H. Muller, AC susceptibility of a monofilament bi-2223/ag superconducting tape in a perpendicular field, Physica C **314**, 183 (1999).

[34] V. Plecháček and F. Gömöry, Magnetic field dependence of critical current density of Bi-Pb-Sr-Ca-Cu-O polycrystalline superconductor, Solid State Commun. **73**, 349 (1990).

[35] P. Fabbricatore, G. Gemme, P. Moreschi, R. Musenich, R. Parodi, and B. Zhang, Determination of the irreversibility line in Bi-2212 Ag sheathed wires, Physica C (Amsterdam, Neth.) **213**, 200 (1993).

[36] A. Gencer, R. H. Mutlu, I. Belenli, Ö. Özogul, and A. Aydinuraz, A study of the nonlinearity in magnetic response of $Bi_2Sr_2CaCu_2O_8$, Supercond. Sci. Technol. **9**, 284 (1996).

[37] R. Prozorov and V. G. Kogan, Effective Demagnetizing Factors of Diamagnetic Samples of Various Shapes, Phys. Rev. Appl. **10**, 014030 (2018).

[38] I. Dhingra and B. K. Das, Frequency, field and thermomagnetic dependence of AC susceptibility in YBCO, Supercond. Sci. Technol. **6**, 765 (1993).

[39] C. N. van Huong, M. Nicolas, J. Negri, and J. P. Burger, Diamagnetism and irreversibility lines in $EuBa_{2-x}K_xCu_3O_7$ compounds, Supercond. Sci. Technol. **4**, 711 (1991).